RSC Advances

PAPER

View Article Online
View Journal | View Issue

Cite this: *RSC Adv.*, 2024, **14**, 32008

Development of *N*-alkylated benzimidazole based cubosome hydrogel for topical treatment of burns†

Maubashera Nawaz,[a] Sofia Hayat,[a] Umer Farooq,[a] Muhammad Adnan Iqbal,*[a] Syed Haroon Khalid,[bc] Tan Wen Nee,[d] Kooi Yeong Khaw,[e] Rabia Munir[b] and Muhammad Umar Ijaz[f]

The current study focuses on assessing the activity of the *N*-alkylated benzimidazole based cubosomal hydrogel (cubogel) for the topical treatment of burn wounds. The study involves the synthesis of six benzimidazole derivatives (**1–6**) and their characterization by FT-IR and ^{1}H and ^{13}C NMR spectroscopy. The further study involves the design and formation of nanoparticles known as cubosomes loaded with selected 1-benzyl-1-benzimidazole (API **6**) and the development of a cubogel for the topical treatment of burn wounds. Cubosomes were prepared by the homogenization method, using glyceryl monooleate (GMO) as a lipid polymer and poloxamer 407 (P407) as a surfactant. Cubosomes undergo *in vitro* characterizations (measurement of particle size, zeta potential, polydispersity index (PDI), % entrapment efficiency, drug release in phosphate buffer saline of pH 6.8, and surface morphology by utilizing TEM (transmission electron microscopy). Formulation D3 (2.5% of GMO, 1% of P407, and 2.5% of PVA) emerged as the optimized formulation, displaying a minimum particle size (PS) of 129.9 ± 1 nm, entrapment efficiency (%EE) of 96.67 ± 0.89%, and a drug release of 86 ± 2.7% at 24 h. Carbopol 940 hydrogel was prepared and incorporated with the optimized formulation to prepare cubogel. This optimized cubogel provided 92.56 ± 0.014% *in vitro* drug release within 24 h. An *in vivo* histopathological study was conducted on an animal model (rabbit) to assess the efficacy of cubogel in wound healing and wound contraction. Then cubogel was compared with the commercially available creams Clotrimazole® and Polyfax®. The wound treated with newly developed cubogel has maximum wound contraction (96.70%) as compared to the standard creams. The findings revealed that the newly formulated cubogel was highly effective in treating burns, showing superior performance to commercial products without inducing side effects. Additionally, benzimidazole derivative loaded cubogel caused a sustained release for treating burn wounds without any bacterial infections. The current results further suggested phase 0 clinical trials.

Received 2nd July 2024
Accepted 18th September 2024

DOI: 10.1039/d4ra04816d

rsc.li/rsc-advances

Introduction

Burns are the 7th universal injury with physical and financial problems for patients and their families, with an estimated 180 000 deaths occurring each year.[1–5] Burns are caused by fire, flame, electric shock, or due to chemicals. The use of topical burn treatment is essential for the survival of patients with severe burns. Burn injuries account for 90% of all injuries in low and middle-income countries (LMICs).[6]

Topical preparations of clotrimazole are used to treat various fungal and bacterial infections. Clotrimazole is an antifungal agent with having broad spectrum of imidazole rings. Clotrimazole-loaded creams or ointments have effective penetration against stratum corneum but their efficiency is limited due to poor penetration, variable drug levels, and poor dermal bioavailability. There is also a major drawback of topical preparations because they cause infection, skin irritation, greasiness, uncontrolled evaporation, and allergic reactions at the infection site.[7]

Benzimidazole is a broad spectrum active pharmaceutical core that possesses pharmacological properties.[8] Benzimidazoles have biological effects such as anti-inflammatory, antioxidant, anti-viral, anti-HIV, anticancer, antibacterial, and antidiabetic.[9–11] Benzimidazole based derivatives (*N*-alkylated) bioactive agents

[a]*Department of Chemistry, University of Agriculture Faisalabad, 38040, Pakistan. E-mail: adnan.iqbal@uaf.edu.pk*

[b]*Department of Pharmaceutics, Government College University Faisalabad, 38000, Pakistan*

[c]*Department of Pharmaceutical Technology, Faculty of Pharmacy, Universiti Teknologi Mara (UiTM), Puncak Alam, 42300, Selangor, Malaysia*

[d]*Chemistry Section, School of Distance Education, Universiti Sains Malaysia, 11800, Malaysia*

[e]*School of Pharmacy, Monash University Malaysia, Jalan Lagoon Selatan, Bandar Sunway 47500, Selangor, Malaysia*

[f]*Department of Zoology, Wildlife and Fisheries, University of Agriculture Faisalabad, 38040, Pakistan*

† Electronic supplementary information (ESI) available. See DOI: https://doi.org/10.1039/d4ra04816d

have drawn much attention in medicinal chemistry such as albendazole, mebendazole, and astemizole.[12] The benzimidazole ring has a significant heterocyclic pharmacophore.[13]

Scientists have been attracted to cubosomes due to the potential drug delivery system which is based on high lipid content, huge surface area, and highly organized arrangement.[14] Cubosomes are lipid-based nanoparticles ranging from 100 to 500 nm, prepared by either dispersing lipid glyceryl monooleate (GMO) in water or micronizing cubic phase in water.[15,16] They have well-defined bicontinuous cubic phase structures with the appropriate amount of water in them.[17] They can encapsulate drugs both hydrophilic and hydrophobic, protect the drugs against physical and chemical degradation, and release the entrapped drug in a sustained manner.[18] Cubosomes enhance the penetration of drugs across the skin layers with almost no observed side effects or irritation.[19] They have applications in both, materials science and medicine.[20]

A secondary vehicle is required to put cubosome into an appropriate and practical topical formulation. This magic is possible through bioabsorbable polymers such as hydrogels. Hydrogels are hydrophilic polymer chains that can hold a large amount of water due to their hydrophilic nature. Therefore, the 3D network of the hydrogel can swell in aqueous media.[21] When cubosomes are loaded into hydrogel it forms cubosomal hydrogel (cubogel). Cubogel is the cubosomal dispersion of hydrogels. The cubosomes enhance the penetration effect across the skin as the structure of cubosomes and stratum corneum are the same.[22,23]

The present research is based on the synthesis of *N*-alkylated benzimidazole (API) based cubosome hydrogel for the topical treatment of burns. API-loaded cubosomes and cubogel formulation were prepared, and characterized through *in vitro* (particle size, zeta potential, %EE, and drug release), and *in vivo* (burn wound treatment, 16 days rabbit model, histopathological evaluation).

Materials and methods

Materials

Benzimidazole, KOH, alkyl halides, chloroform, methanol, ethanol, dimethyl sulfoxide (DMSO), and *n*-hexane were purchased from Sigma Aldrich (St. Louis, USA). GMO was purchased from Macklin Biochemical Co. (Shanghai China). Poloxamer 407 (P407), polyvinyl alcohol (PVA), carbopol 940, and triethanolamine were purchased from Sigma Aldrich (St. Louis, USA). Distilled water (used during experiments) was obtained from the Organometallic and Coordination Chemistry Laboratory, UAF, Pakistan.

Synthesis of *N*-alkylated benzimidazoles

The compounds (**1–6**) were synthesized according to our previously reported method with minor modifications.[24] Benzimidazole (1 equiv), KOH (1.5 equiv), and DMSO (40 mL) were taken in a round bottom flask and stirred at 1200 rpm for 30 minutes at RT. After that alkyl halide (1 equiv) was added dropwise and kept on stirring for 3 h. After stirring, the reaction mixture was added to 300 mL of distilled water. Suddenly turbid white solution appeared, and the reaction mixture was filtered and then washed with DMSO and *n*-hexane. The final product was dried at ambient temperature. The different vibrational bands and NMR signals of these compounds (**1–6**) have been presented in a ESI section.†

Physical properties of APIs

The synthesized API **1–6** were observed physically for their appearances and melting points were measured using SANYO Gallen Kamp, JAPAN, melting point apparatus.

Characterization of APIs

The bonding between benzimidazole and alkyl halide can be studied using Fourier transform infrared (FT-IR) spectroscopy initially. The sample were compressed and placed on the ATR crystal for analysis. The ATR crystal was scanned from 4000 to 650 cm^{-1} using an Agilent Technologies FT-IR spectrophotometer (Cary 630) at the environmental chemistry laboratory, University of Agriculture Faisalabad, Pakistan.

^{1}H and ^{13}C-NMR spectral analyses were performed in $CDCl_3$ solvent with a Bruker 400 MHz ultra-shield machine. δ were recorded in ppm and J values were given in Hz. The signals were labeled as s, d, t, and m, which represent singlet, doublet, triplet, and multiplet, respectively.

Preparation of cubosomes

Cubosomes were prepared according to the previously reported method with slight modifications.[25] The twelve cubosomal dispersions including six blank (without drug, API) and six drug loaded formulations were prepared by homogenization of the lipid phase consisting of GMO and P407 with PVA in water.

The composition of formulations is shown in Table 1. Cubosomes were prepared by melting GMO and P407 on a hot plate at 60 °C, which ensures the components were thoroughly mixed in the liquid state. Simultaneously, PVA was dissolved in

Table 1 Composition of cubosomes both blank and drug loaded formulations

Dispersions	GMO (%)	P407 (%)	PVA (%)	API (%)	Water (mL)
Blank					
B_1	2.5	1	1.5	—	9.5
B_2	2.5	1	2	—	9.45
B_3	2.5	1	2.5	—	9.4
B_4	2.5	0.5	2	—	9.5
B_5	2.5	1	2	—	9.45
B_6	2.5	1.5	2	—	9.4
Drug loaded					
D_1	2.5	1	1.5	1	9.4
D_2	2.5	1	2	1	9.35
D_3	2.5	1	2.5	1	9.3
D_4	2.5	0.5	2	1	9.4
D_5	2.5	1	2	1	9.35
D_6	2.5	1.5	2	1	9.3

distilled water and heated on the same hot plate at the same temperature for 15–20 minutes. Once GMO and P407 were completely mixed the drug was added to this mixture by increasing the temperature up to 100 °C because at this temperature drug mixed well. When PVA was completely dissolved in water then PVA containing distilled water was added dropwise to the drug loaded mixture and the stirring rate increased up to 1100 rpm for half an hour. This vigorous stirring was necessary for achieving a homogeneous mixture. After complete mixing, a yellowish color mixture was obtained. Then it was sonicated using a bath sonicator (ultrasonic cleanser) that helps in breaking down any aggregates and promotes a uniform dispersion. A well-dispersed sample had a turbid whitish consistency and no noticeable aggregates. At the end that sonicated dispersion was homogenized (Heidolph Instruments) at 15 000 rpm for 10 min to obtain the nanosized cubosomes. The bluish-colored dispersion was obtained. The blank formulations follow the same process without the addition of API. The schematic diagram of the formation of cubosomes is given in the ESI Fig. S1.†

Characterization of cubosomes

Fourier-transform infrared (FT-IR). The bonding between the drug and other ingredients of cubosomes can be studied using Fourier transform infrared (FT-IR). The sample of the optimized formulation of cubosome and API, GMO, PVA, and P407 was placed on the ATR crystal for analysis. The ATR crystal was scanned from 4000 to 650 cm^{-1} using an Agilent Technologies FT-IR spectrophotometer (Cary 630) at the environmental chemistry laboratory University of Agriculture Faisalabad, Pakistan.

Characterization of nanoparticle properties: PS, PDI, and ZP. The average particle size (PS) and zeta potential (ZP) of both blank and drug-loaded cubosomal dispersions were accurately determined using the dynamic light scattering (DLS) technique. This analysis was conducted with a computerized Malvern Zetasizer (Malvern Instruments Ltd. Worcestershire, UK) at 25 °C. To facilitate this process, all samples were diluted in distilled water at a ratio of 1 : 10. They were then placed in clear, disposable zeta cells, with measurements taken and recorded at 25 °C.[26] This procedure was replicated three times to ensure reliability, and the results are presented as mean values accompanied by their respective standard deviations.

Determination of entrapment efficiency. Cubosomal formulations were separated from the unentrapped (API **6**) by centrifugation (Hermle Benchmark 2206A) at 6000 rpm for 30 minutes at room temperature.[27] A spectrophotometer was used to determine concentrations of API in the supernatant at predetermined λ_{max} 280 nm. The following equation was used to measure the %EE. The %EE was measured three times, and an average result was determined.

$$\%EE = \frac{(\text{amount of drug added} - \text{amount of drug in supernatant})}{\text{amount of drug added}} \times 100$$

High resolution transmission electron microscope (HR-TEM)-morphology study. The optimized formulation of cubosome D3 was analyzed using a HR-TEM to check the morphology and nano size structure. One drop of the optimized formulation was diluted and placed on the grid. A filter paper was used to absorb the excess solvent. Then, it was left to dry for 3 minutes and examined by HR-TEM (FEI Tecnai G2 20 S-TWIN, 200 kV). The process was conducted at the School of Distance Education, Universiti Sains, Malaysia.

Determination of *in vitro* drug release. *In vitro* drug release was determined by using a dialysis membrane with a molecular weight cut off 12–14 k using pH 6.8 phosphate buffer saline (PBS) containing 1% drug. One mL of D1–D6 formulations was put individually in the dialysis bag and tightly sealed with thread. This sealed membrane was suspended in the beaker 250 mL buffer solution and placed in the shaking water bath (Thermo Scientific-USA) at a maintained temperature of 37 °C and 50 rpm stirring.[28] At different time intervals (10, 20, 30, 40, 60, 120, 180, 240, 300, 360, 420, 480 and 1440) minutes, 5 mL buffer solution was withdrawn and the equal volume of release media was regularly replaced to maintain the sink condition.[29] The amount of API released from cubosome formulation was quantified using a spectrophotometer at a predetermined wavelength of 280 nm. The experiment was performed three times for each formulation, and an average result was determined.

Preparation of cubogel. Cubogel was prepared by the previously reported method with some modifications.[30] The hydrogel was prepared by mixing 1% carbopol 940 in distilled water and allowed to settle the mixture for 24 hours at RT. Then an equal proportion of the optimized formulation was added to carbopol 940 hydrogel. The optimized formulation was added dropwise to the carbopol 940 hydrogel at 1500 rpm stirring. It was performed carefully to ensure even distribution. Triethanolamine (1–2 mL) was added to neutralize the pH of the cubogel to make it suitable for topical application.[22] The schematic diagram of the development of cubogel is given in the ESI Fig. S2.†

Physical appearance of cubogel. The freshly prepared cubogel was under examination visually for physical characteristics *i.e.*, homogeneity, color, and uniform distribution of cubosomes.

pH of cubogel. The pH of the cubogel was determined by using a digital pH meter (HI-9811-5, Hanna Instruments, USA). This is crucial to remove any residual substances from previous measurements that could interfere with the accuracy of the current reading. The electrode was then directly immersed into the cubogel for the pH measurement.[22] The pH was measured three times, and an average result was determined.

Surface morphology of cubogel. The morphology of cubogel was examined using the same method as for the cubosomes. Refer to the section on High-resolution transmission electron microscopy (HR-TEM).

Rheological behavior of cubogel. The investigation of a drug-loaded cubogel encompassed an assessment of rheological behavior and spreadability. The rheological properties of the prepared cubogel were analyzed by Brookfield viscometer (DV-II + Pro) using spindle S 63 at rotation speed 10–100 rpm. A 0.5 g

sample was placed in a falcon tube and diluted to 50 mL. The viscosity was measured in triplicate at RT.[29]

The spreadability of cubogel plays a pivotal role in ensuring the efficacy of topical therapy and the accurate administration of medicinal formulations. The spreadability is contingent upon the flow properties of the formulation.[22] To check the spreadability, a 1 cm diameter circle (D1) was marked on a clean, dry glass slide. Subsequently, 0.5 g of cubogel was carefully applied within the circle, ensuring no spillage beyond its boundaries. Another glass slide was placed on top to cover the cubogel-loaded slide, and various weights (ranging from 100 to 500 g) were applied.[31] Following this procedure, the cubogel shifted from its initial position (D1) to a new location (D2), indicative of its spreadability characteristics.

Skin irritation test. The potential for localized skin reactions of cubogel was evaluated using a skin irritancy test. The test involved dividing the shaved skin of a rabbit into two distinct patches. Cubogel was applied to one patch, while the other was served as a negative control with no application. Over 48 hours, both patches were closely monitored for any signs of irritation, such as erythema. The skin irritation observed in both groups was observed using the Draize scale.[32–34]

Burn wound healing of cubogel

Animal model. The Research Ethics Committee (Research Innovations & Commercialization) accepted the study guidelines under letter number (4090/ORIC, 24/7/2023) at the University of Agriculture Faisalabad, Pakistan (Fig. S3 Bioethics certificate, see ESI†). The animals were handled according to the recommendation of ethics guidelines of The National Biosafety Rules of 2005, the Punjab Biosafety Rules of 2014, the Punjab Animal Health Act of 2019, and the Bioethics Protocol. The study was carried out on three female rabbits (aged 5–8 months), weighing between 1 and 1.5 kg. The animals were clinically healthy with no skin wounds. The animals were housed in separate cages at room temperature with controlled humidity levels and fed with a normal diet (grass, fruits, vegetables) and water.

Inducing burn wound. The rabbits were purchased from the market and kept in cages for 2–3 days to acclimatize. It is necessary for reducing stress and allowing the animals to adjust to the new environment, which can influence physiological responses and the accuracy of the study results. The wound model was made with slight modifications to the previously reported method.[35] The back of the rabbits was shaved by using VEET® cream, shaving was necessary to expose the skin to burn. The next day, six marks were placed on their back, these marks indicated where the burn wounds would be created. These marks were injected with Xyloaid® to numb them and reduce the pain during the wound creation process. The iron metal stamp (1.5 × 1.5 cm in diameter) was used to create the burn wounds. The use of standardized size and shape ensures consistency in the wounds across different treatments. The metal stamp was heated in an oven at 80 °C and the heated iron metal stamp to the predetermined area for the specified duration of 14 seconds to induce the burn.[36] The schematic diagram of the burn induction method is given in the ESI Fig. S4.†

Assessment of burn wound healing. According to the wound model, six burn wounds (I, II, III, IV, V, VI) were induced. After that cubogel and reference creams were applied daily to the wounds. All the wounds were closely observed for any infection. Wounds I, II, and III were treated with cubogel, IV treated with Clotrimazole®, V treated with Polyfax®, and VI left untreated. All wounds were photographed daily and each wound was measured daily with a ruler to determine how well it had healed. The area of each wound was calculated by using the given equation.

$$\text{Wound closure} = \frac{\text{wound area on day } 0 - \text{wound area on } n\text{th day}}{\text{wound area on day } 0} \times 100$$

After 16 days of study, the rabbits were slaughtered and skin samples were taken for histopathology study.

Assessment of epithelialization. The topical formulations of cubogel and the marketed creams Clotrimazole® cream 20 g (Clotrimazole 1% w/w) and Polyfax® (20 g skin ointment) were applied to the inflicted wound areas of rabbits from day 1 to day 16. Application of each cream and gel was continued for 16 days, once a time daily. The number of days needed for the eschar to peel off the burn site surface without leaving a raw wound behind was used to track the epithelialization process.[30]

Histopathology. After 16 days the histopathological study was performed according to the reported method with some modifications.[37] The infected skin patches were taken and fixed in 10% formalin solution for 24 h. The patches were embedded in paraffin after dehydrating. Each patch was sectioned at 5 μm thickness and stained with hematoxylin and Eosin (H & E) for examination by light microscopy.

Results and discussion

Synthesis of APIs

The general procedure that involves the synthesis of APIs is shown in Scheme 1. Potassium hydroxide was added to the solution of benzimidazole in DMSO at room temperature. Respective alkyl halide was added dropwise in the same reaction medium. Since the reaction medium is exothermic a dropwise addition of alkyl halide was strictly followed and the flask was

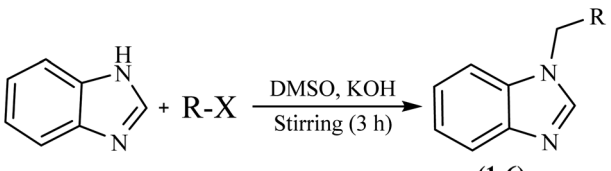

(1-6)

R	R
1. Ethyl	4. Pentyl
2. Propyl	5. Hexyl
3. Butyl	6.Benzyl

Scheme 1 Synthesis of *N*-alkylated benzimidazoles (APIs).

placed in a water bath to dissipate the heat. In the case of benzyl bromide (alkyl halide), the procedure was done in the fume hood to avoid the eye irritation of the benzyl bromide. The reaction mixture was stirred for 3 h at room temperature and was then poured into 300 mL of distilled water. If the oily liquid mixture was obtained after stirring then it was extracted with chloroform and the combined extract was filtered through Whatman filter paper. The process of filtration was repeated twice. The filtered compound was obtained as a thick yellowish fluid. If some solid particles are shown at the bottom of the flask after stirring. Then the product was filtered and washed with DMSO and *n*-hexane, and dried at room temperature. The product appeared as a white shiny powder. Both were safely stored in the Eppendorf for further characterization and activities.

Characterization of APIs

Physical properties. The six API were prepared and their physical properties were examined shown in Table 2.

All these APIs were prepared according to the previously reported method.[38,39] According to the preliminary study, from all synthesized compounds API **6** showed the best antibacterial activity. So, in this study API **6** was incorporated into the cubosomes and cubogel, to check the antibacterial activity and burn wound healing. According to best of our knowledge, there is no commercially available topical formulation of benzimidazole that provides sustained release at this time.

FT-IR spectroscopy. FT-IR spectral features of all the synthesized compounds were observed using the ATR over the scan range of 4000 to 650 cm^{-1}. The results show that after alkylation the spectral features of benzimidazole changed compared to the unreacted benzimidazole. For example, a broad vibrational band of 2500–3200 cm^{-1} of benzimidazole split into two distinguishable bands; (i) 2750–2950 cm^{-1} for the alkyl chain (C_{sp^3}–H) and, (ii) 3000–3100 cm^{-1} for an aromatic ring (C_{sp^2}–H) in *N*-alkyl benzimidazole. This splitting provided preliminary indications for the successful *N*-alkylation of benzimidazole moiety.[40–42] Fig. S4.† FT-IR spectrum of API **6** (1-benzyl-1-benzoimidazole), see ESI.†

NMR studies of APIs. NMR spectra of all synthesized compounds have been analyzed either in $CDCl_3$-d_3 or DMSO-d_6 over the scan range 0–16 δ ppm for ^{1}H NMR and 0–200 δ ppm for ^{13}C NMR studies. The attachment of respective alkyl halides with benzimidazole to get *N*-alkylbenzimidazoles (**1–6**) was confirmed by observing changes in specific chemical shifts of alkyl halides and *N*-alkylbenzimidazoles. For example, the downfield movement of signal (triplet) from δ 3.21 (of propyl bromide) to δ 4.10 (in *N*-propylbenzimidazole) and the appearance of a new signal in the range δ 7.00–8.00 for aromatic protons supported the successful attachment of both the reactant. In ^{13}C NMR spectra, similar changes can be observed leading to the confirmation of targeted *N*-alkylbenzimidazole. All alkyl (ethyl, propyl, butyl, pentyl, and hexyl) substituted benzimidazoles show parallel changes in chemical shifts according to the previously reported results.[42–44]

^{1}H-NMR spectrum of the selected API **6** showed the various protons in different chemical environments see Fig. 1a. ^{1}H-NMR spectrum showed a sharp singlet proton of benzyl group CH_2 resonated at 5.32 δ ppm indicating a successful *N*-alkylation. The chemical shifts in the range δ ppm 7.21–7.80 indicate an aromatic (CH) presence, while the signal at the downfield region, δ H 7.93 ppm, corresponds to the proton on the $C_7H_5N_2$ frame NCHN. In the ^{13}C NMR spectrum of API **6**, Fig. 1b, the CH_2 carbon of the benzyl group appeared at δ 48.8 and the C_{aliph} appeared at δ 143.1 ppm. The remaining carbons appeared in the range of δ 110.0–143.9 ppm.[45–48]

Formulation of cubosomes. The formulation process of cubosomes involved a careful sequence to create lipid-based dispersions. GMO was used in the formulation of cubosomes.[49] The amphiphilic nature of GMO allows the incorporation of both hydrophobic and lipophilic drugs (API).[50] The formulation was followed by the gradual addition of P407, which formed an aqua color mixture, where GMO was used for the nanostructure system[51] and P407 and PVA acted as a surfactant and stabilizer.[52] The stabilizer was used to ensure the stability of the dispersed system.[17] The presence of PVA molecules in the solution hinders the aggregation of nanoparticles by forming a protective layer around them due to steric repulsion. As a result, the nanoparticles remain dispersed in the solution and undergo controlled growth, leading to the generation of smaller particles with a uniform size distribution. The use of PVA dissolved in distilled water and heating is an important step. PVA acts as a stabilizing agent, which is essential in maintaining the integrity of the cubosomes and preventing aggregation. The addition of the drug at a higher temperature (100 °C) was indicated that the drug used has specific solubility characteristics, necessitating a higher temperature to achieve an effective mix. This step was crucial for drug-loaded formulations and influences the efficacy of drug encapsulation and subsequent release. The vigorous stirring at 1100 rpm and sonication was a key to achieving a homogeneous mixture and reducing particle size. Sonication, in particular, helps break down aggregates, ensuring uniform dispersion and stability of the cubosomes. The change in color from yellowish to a turbid white consistency upon sonication, followed by a bluish color after homogenization,[53] could indicate the formation of cubosomes and might be used as a visual cue for the successful preparation of the dispersion. The final step of homogenization at 15 000 rpm[49] for 10 minutes to achieve nanosized cubosomes was crucial. This high-shear process was responsible for reducing the particle size to the nanoscale, which is essential for the desired drug release profile and bioavailability.

Table 2 Physical properties of APIs

API	Name	Appearance	MP/BP (°C)
1	*N*-Ethyl benzimidazole	Colorless, thick fluid	184–186
2	*N*-Propyl benzimidazole	Colorless	236–238
3	*N*-Butyl benzimidazole	Yellow liquid	256–258
4	*N*-Pentyl benzimidazole	Thick yellowish liquid	262–263
5	*N*-Hexyl benzimidazole	Thick yellowish fluid	270–275
6	*N*-Benzyl benzimidazole	White shiny powder, solid	110–120

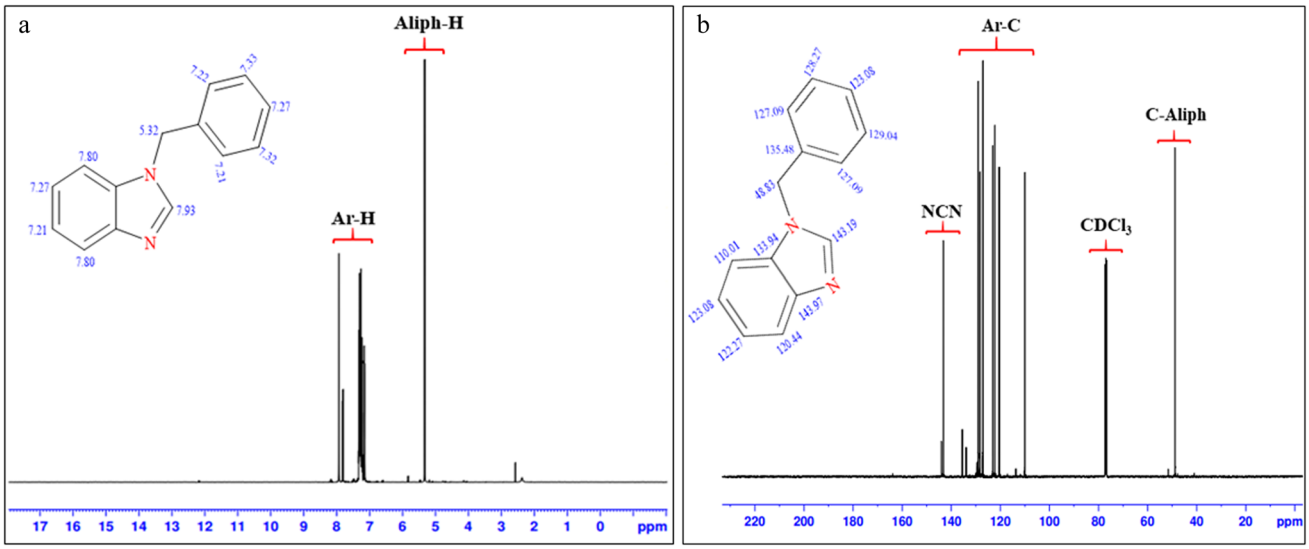

Fig. 1 ^{1}H NMR (a) and ^{13}C NMR (b) spectrum of *N*-alkylated of benzimidazole.

Characterization of cubosomes

FT-IR spectroscopic analysis of cubosomes. Cubosomes and lipid interaction were studied by FT-IR analysis Fig. 2[a]. FT-IR may predict the chemical interaction and stability of API with other bulking agents present in the cubosomes.[54] FT-IR spectrum of *N*-alkylated benzimidazole showed stretching peaks at 3080–3020 (C–H_{arom}), 1670–1610 (C=N),[55] 1591–1522 (C=C). The peaks of *N*-alkylated benzimidazoles were shown in the spectrum of the physical mixture indicating no interference between the drug and other bulking agents. The disappearance of the drug peaks from the cubosome spectrum indicated its solubilization within the cubosomal matrix[56] are given in Table 3 and Fig. 2[a].

The drug characteristic speaks are not visible in cubosomes spectrum suggesting that the drug is well integrated into the matrix, possibly to non-covalent interaction like hydrogen bonding or van der walls forces. The characteristics peak of interaction between *N*-alkylated benzimidazole loaded cubosomes and their bulking agent are given in Table 3 and Fig. 2[a]. Interestingly some peaks of bulking agent are still prominent in the cubosomes (Table 3).

The physicochemical properties of cubosomes were analyzed in the nano range and are shown in Table 4 the particle size of the blank and drug loaded cubo ranged from 120.8 ± 1.656 to 180.1 ± 2.645 nm and 129.9 ± 1 to 177.2 ± 1.509 nm, respectively (Fig. 2[e]). Upon loading with *N*-alkylated benzimidazole, it could be seen that the average particle size is decreased[54] due to the amphiphilic nature of API **6**.[61] PDI is also decreased when the drug is loaded ranging from 0.344 ± 0.001 to 0.483 ± 0.005 and 0.309 ± 0.005 to 0.421 ± 0.001 of blank and drug loaded cubosomes, respectively. The results of PDI mono dispersity of drug loaded cubosomes approach zero. The range of zeta potential is ±30 for the physical stability of formulations.[61] The blank and drug loaded cubosomes were negatively charged with a zeta potential of −10.6 ± 0.152 to −18.9 ± 0.950 and −14.3 ± 1.873 to −18.3 ± 1.442, respectively and shown in Fig. 2[g]. Therefore, the zeta potential of these cubosomes indicates their physical stability.

Table 3 Characteristics peaks of cubosomes and its bulking agents

Compounds	–OH (cm^{-1})	–C=O	–CH	–C=N	Ref.
(a) API **6**	—	—	3080	1610	55
(b) Cubosomes	3315	1636	—	—	57
(c) GMO	—	1740	2920	—	58 and 59
(d) Poloxamer 407	—	1099	2968	—	59
(e) PVA	3309	—	2905	—	60

The particle size and zeta potential are crucial factors influencing the biopharmaceutical properties, drug release, entrapment efficiency, and stability of nanoparticles. These characteristics are largely determined by the concentrations of P407 and polyvinyl alcohol (PVA). The zeta potential is relatively low due to the presence of nonionic surfactant, which enhances stability by providing steric hindrance, thus preventing aggregation during storage.[62,63] The data presented in Table 4 elucidates the significant impact of P407 and PVA concentrations on the particle size, zeta potential, and polydispersity index of cubosomes. In dispersions 1–3, the concentration of P407 was kept constant, while the PVA concentration was increased from 1.5% to 2.5% for both blank and drug-loaded cubosomes. This increase in PVA concentration correlated with a decrease in particle size.[64] Conversely, in dispersions 4–6, the concentration of PVA was constant, and the P407 concentration was varied between 0.5% and 1.5%. This variation resulted in a notable decrease in the average particle size of the cubosomes as the P407 concentration increased, as detailed in the study.[64] Throughout all these dispersions, the concentration of GMO remained unchanged, ensuring a consistent lipid content in the formulations.

Transmission electron microscopy (morphology). Transmission electron microscopy (TEM) analysis of the optimized cubosomal formulation D3 unveiled its cubic nano size. In Fig. 2[c], [f] and [h] the particles exhibit clear separation,

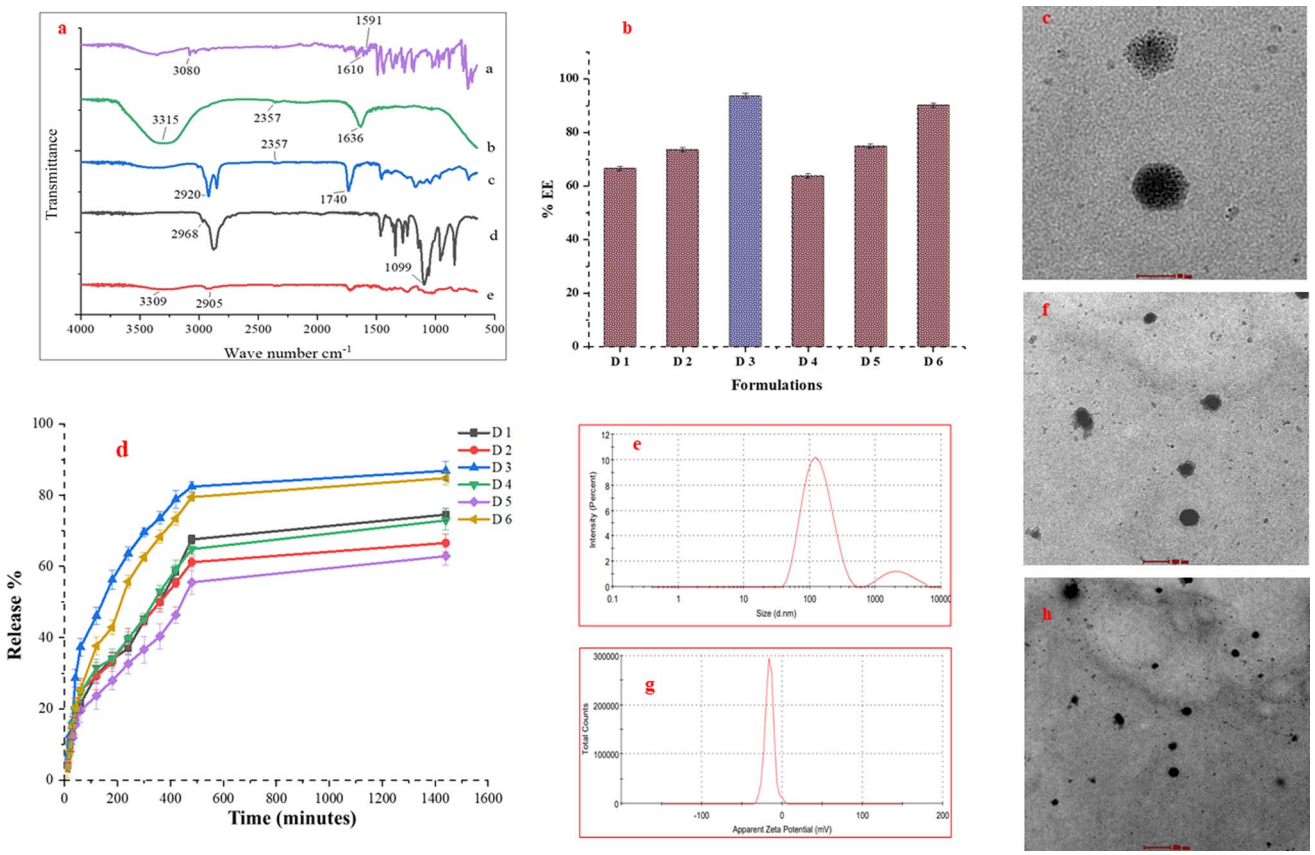

Fig. 2 [a] FT-IR spectra of (a) API **6**, (b) cubosomes, (c) GMO (d) P407, and (e) PVA. [b] Entrapment efficiency of all the cubosomal formulations (D1-D6). [c], [f] and [h] are TEM images of optimized cubosomes by 50 nm, 100 nm and 200 nm resolutions respectively. [d] Drug release of all the formulations of cubosomes (D1–D6). [e] Particle size and [g] Zeta potential of optimized cubosomes.

confirming their nano dimensions, as previously determined by the Malvern Zetasizer (129 nm). Based on the current results particles falling within the 100–200 nm range, indicating consistent size characteristics. Particularly, a uniform dispersion of particles across the formulation is observed. TEM examination further explained that the nanoparticles possess nearly cubic shapes, demonstrating uniform size distribution and smooth surfaces.

Entrapment efficiency (%EE). %EE is a key parameter in drug delivery systems, measuring the percentage of a drug that is successfully encapsulated within the delivery vehicle (cubosomes) compared to the total amount of drug used. The EE of API **6** loaded cubosomes ranged from 63% to 93% indicating the variation in the efficiency of drug encapsulation among all the formulations. Fig. 2[b] and Table 4 show the successful entrapment of API **6** into cubosomes. P407 and PVA created

Table 4 The characteristic properties of formulated cubosomes[a]

Dispersions	PS (nm)	ZP	PDI	%EE	Drug release
B_1	120.8 ± 1.656	−10.6 ± 0.152	0.358 ± 0.006	—	—
B_2	180.1 ± 2.645	−14.4 ± 1.250	0.483 ± 0.009	—	—
B_3	133.9 ± 2.645	−18.9 ± 0.950	0.426 ± 0.001	—	—
B_4	154.8 ± 2.722	−11.1 ± 1.517	0.344 ± 0.001	—	—
B_5	180.1 ± 2.645	−14.4 ± 1.250	0.483 ± 0.005	—	—
B_6	175.1 ± 3.194	−14.3 ± 1.582	0.477 ± 0.002	—	—
D_1	170.3 ± 2.475	−17.2 ± 1.527	0.421 ± 0.001	66.59 ± 0.81	74 ± 1.8
D_2	167.4 ± 2.608	−14.3 ± 1.873	0.378 ± 0.002	73.53 ± 0.83	66 ± 2.5
D_3	129.9 ± 1	−16.3 ± 1.715	0.309 ± 0.005	93.67 ± 0.89	86 ± 2.7
D_4	177.2 ± 1.509	−18.3 ± 1.442	0.398 ± 0.003	63.81 ± 0.84	72 ± 2.7
D_5	167.4 ± 2.514	−14.3 ± 1.873	0.378 ± 0.003	74.92 ± 0.81	62 ± 2.5
D_6	134.8 ± 1.900	−18.2 ± 1.562	0.374 ± 0.003	90.27 ± 0.82	84 ± 1.8

[a] Effect of P407, PVA, and GMO on PS, ZP, PDI.

a layer on top of the cubosomal nanovesicles, which stabilized the cubosomal dispersion. This stabilization is important because it helps to retain the maximum amount of API **6**, which raises the %EE.[65] The high encapsulation of the lipophilic drug in the cubosomes is attributed to the attraction between the lipophilic parts of the cubosomal bilayer and the lipophilic nature of the drug.[66] Due to this reason, D3 (93%) and D6 (90%) show the highest percentage of EE as they contain high amounts of P407 and PVA. The values of %EE were arranged as follows: D3 > D6 > D5 > D2 > D1 > D4.

***In vitro* drug release.** The *in vitro* drug release study of cubosomes loaded with API was determined using the diffusion technique of dialysis membrane (12–14 kDa, molecular weight cutoff), for 24 h. Using the dialysis bag approach, *in vitro* release assays were conducted in 6.8 pH phosphate buffer containing 10% ethanol to release the drug that was entrapped within cubosomes. The amount of cubosome containing at least 1 mg drug API **6** was incorporated into the dialysis bag and immersed in 250 mL release medium (composed of 90% PBS pH 6.8, and 10% ethanol). The release study was done in a shaking water bath (Thermo Scientific-USA) at 37 °C with 50 rpm rotation. A biphasic release pattern was visible where initial burst release occurs within 2 hours followed by a sustained release during 24 hours from cubosomes. The burst release was seen during the first 2 hours caused by the unentrapped drug. Following this burst phase, the entrapped cubosomes released the drug in a steady pattern. The drug release after 2 hours was 26%, 29%, 46%, 31%, 23%, and 37% of D1–D6 respectively Fig. 2[d]. There is a clinical importance of biphasic pattern as the 1st burst release starts a rapid action while a long-time slow release allows the drug to manage for a long time.[25] After 24 hours the drug release of D1–D6 was 74%, 66%, 86%, 72%, 62%, and 82% respectively. After 24 hours, a maximum sustained drug release of 86% was noted in the formulation D3 which was selected as the optimized formulation. According to these results, the drug that was adsorbed on the cubosome surface caused the first burst effect, but the drug that was trapped inside the cubosomes caused the continuous release performance.[67]

Selection of optimized formulation. The selection of the optimized formulation was based on criteria such as the smallest particle size (within the range of less than 200 to 300 nm), the highest EE, and prolonged drug release lasting up to 24 hours. Formulation D3, comprising 2.5% of GMO, 1% w/w of P407, and 2.5% w/w PVA, emerged as the ideal choice. This formulation demonstrated a minimal particle size of 129.9 nm, an impressive EE of 96.67%, and sustained drug release of 86% at the 24 hour mark. These attributes were achieved within

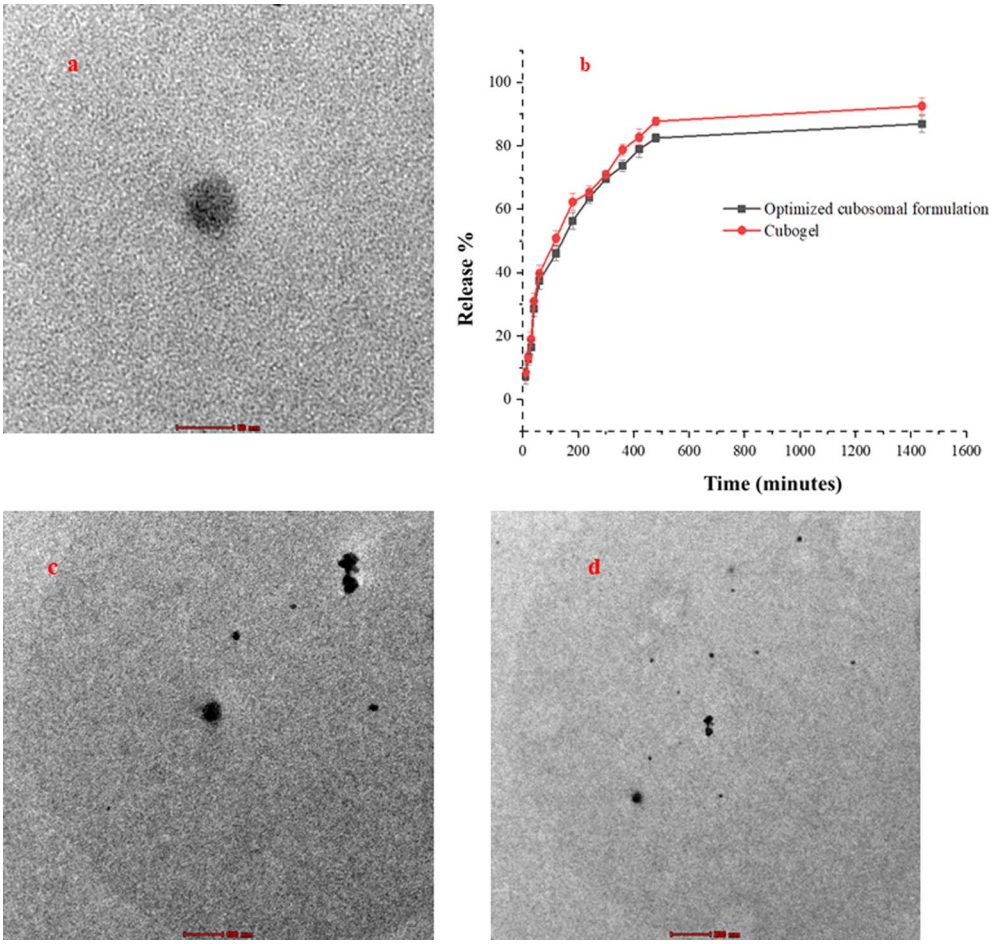

Fig. 3 (a), (c), and (d) images of cubogel taken by HR-TEM at 50, 100 and 200 nm resolutions. (b) The *in vitro* drug release of optimized cubosomal formulation compared to cubogel at 37 ± 0.5 °C.

a design space characterized by a desirability value of one. Following this successful optimization, formulation D3 was then utilized in the formation of the cubogel.

Characterization of cubogel

Development of cubogel. The general scheme of the development of cubogel, see the ESI.† The previously reported method[30,68] is used with some modifications. The preparation of cubogel involves a combination of carbopol 940 and drug-loaded cubosomal dispersion. Carbopol 940 is a synthetic polymer that is effective for creating gels. The 24 hour waiting period at room temperature was necessary for the gel formation. This time allows the carbopol 940 hydrogel to fully swell and entangle, to escape air bubbles resulting in a gel with the desired consistency and viscosity.[30,69] This combination aims to power the benefits of both systems, the stability and consistency of cubogel, and the drug delivery capabilities of cubosomes. Adding the cubosomal dispersion dropwise at 1500 rpm ensures a uniform distribution of the cubosomes within the gel matrix.[70,71] This is important for maintaining the stability of the cubosomes and ensuring an even distribution of the drug within the gel. The addition of triethanolamine for neutralization is an important step. Cubogel is typically acidic, and neutralization is necessary to increase the pH to a more skin-friendly level. Triethanolamine serves not only to adjust the pH but also to enhance the cubogel properties, such as viscosity and clarity.

Table 5 Viscosity of cubogel

Rpm	Viscosity of cubogel
10	3300 ± 0.12
20	2593 ± 0.14
50	2020 ± 0.11
100	1265 ± 0.13

Physical appearance. The appearance of cubogel was light yellowish in color and translucent. This slight tint might be a result of the API **6**. The formulation was found to be smooth which is a desirable quality for a gel especially when it is used for a topical application and free from granules which indicates an effective homogenous mixture.[30]

The pH of the cubogel formulation was determined to be in the range of 5.0 to 5.3, indicating its suitability for topical application due to its compatible pH range.[72,73] It aligns with the natural pH of the skin, reducing the risk of irritation and ensuring compatibility.

Morphology of cubogel. The TEM images of the cubogel indicated the nano vesicular cubic shape with uniform nano size in Fig. 3a, c, and d compared to the TEM of the optimized cubosomal formulation D3.

Rheological behavior of cubogel. The viscosity of the prepared cubogel is displayed in Table 5. The viscosity of the prepared cubogel is a parameter essential in evaluating the rheological properties of cubogel formulations. These properties, including viscosity, significantly influence the physical form, appearance, texture, and flow behavior of the product. The study reveals that hydrogel loaded with cubosomes exhibits shear-thinning behavior, characterized by a decrease in viscosity with an increasing shear rate.[74] Specifically, the viscosity of the cubogel was measured within a range of 1265 to 3300 cps, affirming their shear-thinning nature. These findings underline the dynamic viscosity characteristics of cubogel under varying shear rates, an important consideration for their application and performance in a gel-based formulation.

Skin irritation test. It was necessary to consider the skin irritation potential after topical application as the cubogel was made of lipid, surfactant, and stabilizer. The recorded zero scores for the cubogel (by visual examination) indicate the absence of any dermal irritation. No clear erythema or edema was observed on the rabbits' skin after application for two days.

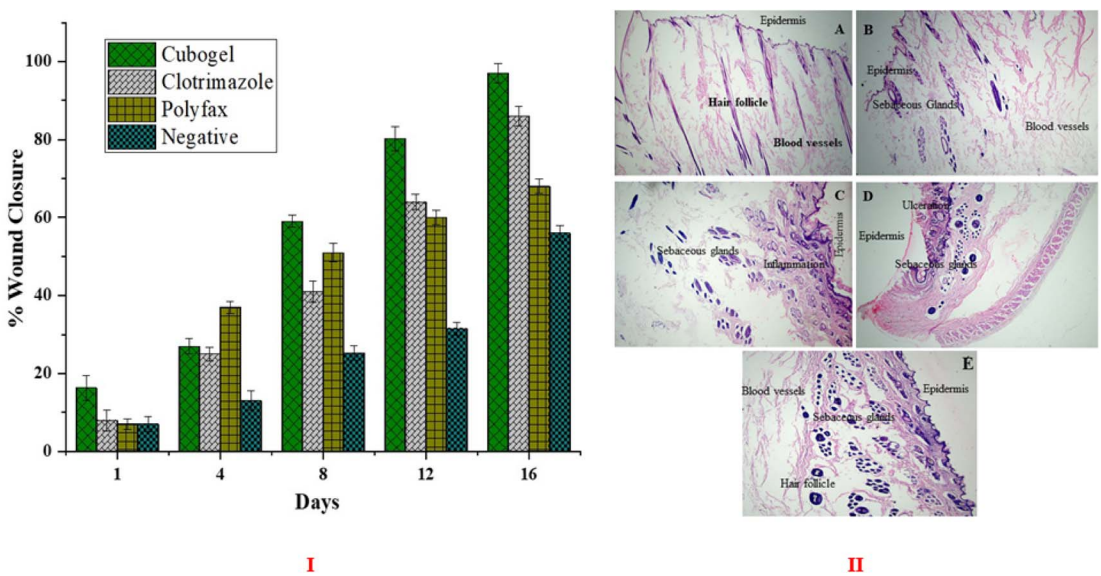

Fig. 4 (I) % Wound contraction of cubogel, standards (Clotrimazole® and Polyfax®), and control groups at the 1st, 4th, 8th, 12th, and 16th day. (II) Histopathological examination of Rabbit's skin. The basic structure of normal skin (A). Untreated wound (B). The wound was treated with clotrimazole® (C). The wound was treated with Polyfax® (D). The wound was treated with API **6** loaded cubogel (E).

It showed that the cubogel caused no irritation and was accepted for the topical application.

Drug release of cubogel. The *in vitro* drug diffusion study of cubogel was determined using the diffusion technique of dialysis membrane (12–14 kDa, molecular weight cutoff), for 24 h. The amount of cubogel containing at least 10 mg API was incorporated into the dialysis bag and immersed in 250 mL release medium (composed of 90% PBS pH 6.8, and 10% ethanol). The release study was done in a shaking water bath (Thermo Scientific-USA) at 37 °C with 50 rpm rotation. It was found that the cubogel had a drug release of 92.56 ± 0.014% after 24 h, while in the early 5 h, burst release was obtained with 70% drug diffusion. In contrast, the optimized batch (D3) had a drug release of 86% see Fig. 3b. So, it is concluded that the loading of cubosomes into a hydrogel (secondary vehicle) had a positive impact on % drug release.

Assessment of burn wound healing. This study on burn wound healing explores different treatments and their effectiveness in promoting wound closure and healing. The findings suggest a variety of responses to the treatments, with the API **6** loaded cubogel showing particularly favorable results. The wound healing occurs predominantly through wound contraction, a process where the edges of the wound pull towards each other, reducing the wound size. This is a common mechanism in burn healing. There was no inflammation, pus formation, or deterioration of the wound observed during the 16 day study period (Fig. 5). These were the positive signs indicating effective healing without complications.

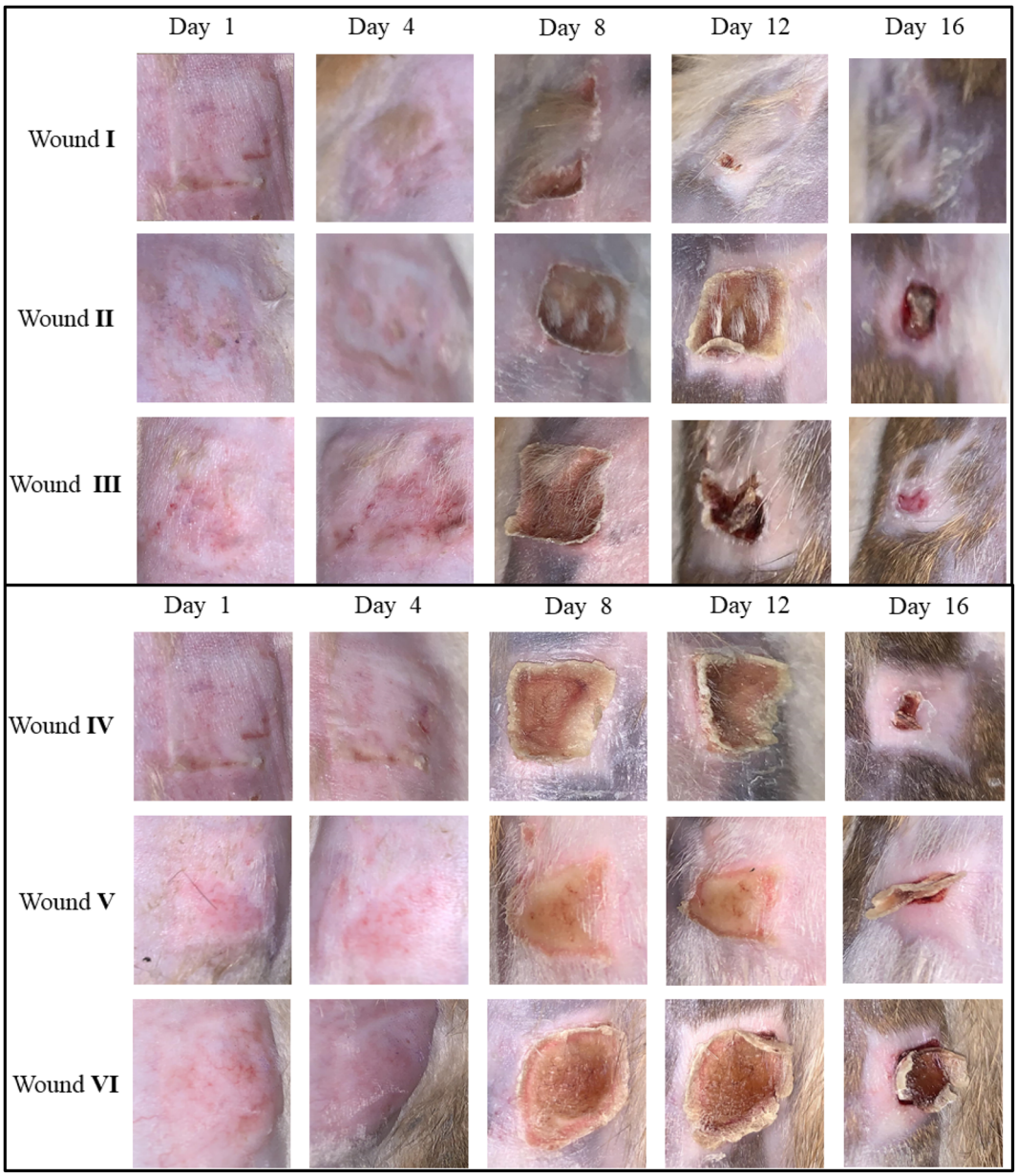

Fig. 5 *In vivo* burn healing study. Wounds I, II, and III were treated with cubogel in a triplicate manner. Wounds IV and V were treated with marketed creams Clotrimazole® and Polyfax® respectively. Wound VI remains untreated.

Efficacy of API loaded cubogel. The cubogel loaded with 1-benzyl-1-benzoimidazole demonstrated the highest percentage of wound closure compared to other treatment groups across all days. The wound I was healed completely in 12 days. Wounds II and III were completely healed after 16 days. This indicates its effectiveness in promoting wound healing. Its success is attributed to the properties of both the active ingredient (API **6**) and the cubosomal formulation, which provides a sustained release of the drug, reducing the need for frequent re-application and minimizing irritation.

Comparison with other treatments. Clotrimazole and polyfax were used in the study, these caused irritation when applied to the burn wound, unlike the cubogel formulation. Wound I, treated with cubogel, completely healed 12th day, showing the skin visible and indicating 100% healing. Wounds II and III were also treated with cubogel, which also healed but took slightly longer, achieving complete healing by the 16th day with healing percentages of 96% and 95%, respectively. Wound IV, with 86% healing, was less effective compared to the cubogel, potentially due to the poor water solubility of clotrimazole and low skin retention of its topical products present a hindrance to the local availability and effectiveness of this drug. Polyfax, another treatment applied to wound V, showed lower healing effectiveness (68%) than both cubogel and clotrimazole by the 16th day. Wound VI, which received no treatment, demonstrated the least healing with only 56% after 16 days see Fig. 4(I).

Implications of the cubogel findings. These results represent the effectiveness of the API **6** loaded cubogel in promoting burn wound healing. Its ability to heal wounds more rapidly and effectively than other treatments, coupled with its non-irritating nature, makes it a promising option for burn care.

The study also highlights the importance of sustained drug release in wound treatment, which can enhance healing and reduce discomfort. The comparative analysis of different treatments provides valuable insights into the efficacy of various therapeutic approaches in managing burn wounds.

Histopathology. To maintain the strength of the skin, wound healing is a controlled complex repair process. Re-epithelization is the most important factor in the wound closure process which identifies the wound healing efficiency. Re-epithelization develops granular tissues at the damaged part of the wound.[26] Histopathological examination was directed to examine the healing process Fig. 4(II). Histopathological examination of the normal skin Fig. 4(II)A of rabbit showed a basic structure of skin with a uniform epidermis, dermis, and hair follicles. This Fig. 4(II)B was subjected to the negative control, which remained untreated during the study showing the epidermis, sebaceous glands, and hair follicle in the developing phase which ensures the rabbit also had some ability to heal itself. The standard clotrimazole Fig. 4(II)C showed incomplete development of the epidermis and the presence of inflammation in the dermis. The other standard polyfax Fig. 4(II)D showed ulceration in the dermis and developing new blood vessels. The results Fig. 4(II)E showed that the wound treated with cubogel had a successful process of re-epithelization due to newly formed blood vessels, formulation of granular tissues, presence of sebaceous glands, and developing process of hair follicles. This wound of rabbit showed a higher rate of wound healing than the other wounds and showed resemblance with the normal skin patch (Fig. 4).

Conclusion

This study presents significant findings in the context of synthesis of benzimidazole derivatives and development of benzimidazole based cubosomes for the topical treatment of burns. It demonstrating the superior efficacy of API **6** loaded cubogel in promoting rapid and effective wound healing without causing irritation or other complications. In conclusion, this research successfully synthesized API **6**, as benzimidazole derivative. Then benzimidazole derivative was incorporated into cubosome formulations that cause a sustained release in treating bacterial infections and burn wounds. The cubosomes, characterized by their small particle size, high entrapment efficiency, and drug release, were effectively integrated into a cubogel for topical application. This cubogel demonstrated remarkable efficacy in burn wound healing, in *in vivo* trials without causing adverse effects. As compared to commercial products (Clotrimazole® and Polyfax®) which cause inflammation and irritation to the burn wounds. The sustained release is characteristic of the cubosomal formulation and plays an important role in its effectiveness. Histopathological evaluations further emphasized the therapeutic potential of formulated cubogel in enhancing effective wound healing. These results have important implications for the development of more efficient and patient-friendly treatments for burn wounds. These findings highlight the potential of this innovative formulation as a superior alternative for burn wound management, showing a significant advancement in the pharmaceutical applications of benzimidazole derivatives.

Abbreviation

API	Active pharmaceutical ingredient
FT-IR	Fourier transform infrared spectroscopy
NMR	Nuclear magnetic resonance
GMO	Glyceryl monooleate
PVA	Polyvinyl alcohol
P407	Poloxamer 407
TEM	Transmission electron microscopy
D	Drug
B	Blank
UAF	University of Agriculture Faisalabad
EE	Entrapment efficiency
PS	Particle size
ZP	Zeta potential
PDI	Polydispersity index
RT	Room temperature

Ethical statement

All animal procedures were performed in accordance with the Guidelines for Care and Use of Laboratory Animals of National

Biosafety Rules 2005, Punjab Biosafety Rules 2014, Punjab Animal Health Act 2019, and Bio-ethics protocols and approved by the Animal Ethics Committee of Chairman Institutional Biosafety and Bioethics Committee (IBC), ORIC at the University of Agriculture Faisalabad, Faisalabad-Pakistan.

Data availability

All the data produced or examined during this research have been provided within the manuscript and ESI.†

Conflicts of interest

All the author declares that there is no conflict of interest in publish this research.

Acknowledgements

The authors are thankful to Pakistan Science Foundation (PSF) for awarding Research grant PSF/CRP/Consrm-676. The authors are thankful to University of Agriculture Faisalabad and Pakistan Science Foundation (PSF).

References

1 E. Siddiqui, N. Zia, A. Feroze, S. Awan, A. L. Ali, J. A. Razzak, A. A. Hyder and A. Latif, *BMC Emerg. Med.*, 2015, **15**, 1–7.
2 A. Wardhana, A. Basuki, A. D. H. Prameswara, D. N. Rizkita, A. A. Andarie and A. F. Canintika, *Burns Open*, 2017, **1**, 67–73.
3 M. F. Sanchez, S. A. Breda, E. A. Soria, L. I. Tártara, R. H. Manzo and M. E. Olivera, *Drug Delivery Transl. Res.*, 2018, **8**, 1000–1013.
4 L. S. Campos, M. F. Mansilla and A. M. M. de la Chica, *Rev. Enfermería*, 2005, **28**, 67–70.
5 W. W. Monafo and M. A. West, *Drugs*, 1990, **40**, 364–373.
6 C. Jacobs, J. Vacek, B. Many, M. Bouchard and F. Abdullah, *J. Surg. Res.*, 2021, **257**, 442–448.
7 P. K. Bolla, C. A. Meraz, V. A. Rodriguez, I. Deaguero, M. Singh, V. K. Yellepeddi and J. Renukuntla, *Molecules*, 2019, **24**, 3139.
8 Y. Li, X. Zhou, H. Wu, Z. Yu, H. Li and S. Yang, *Ind. Crops Prod.*, 2020, **150**, 112406.
9 G. Yadav and S. Ganguly, *Eur. J. Med. Chem.*, 2015, **97**, 419–443.
10 Y. Bansal and O. Silakari, *Bioorg. Med. Chem.*, 2012, **20**, 6208–6236.
11 M. Gaba, S. Singh and C. Mohan, *Eur. J. Med. Chem.*, 2014, **76**, 494–505.
12 L. Zhang, D. Addla, J. Ponmani, A. Wang, D. Xie, Y.-N. Wang, S.-L. Zhang, R.-X. Geng, G.-X. Cai and S. Li, *Eur. J. Med. Chem.*, 2016, **111**, 160–182.
13 N. Singh, A. Pandurangan, K. Rana, P. Anand, A. Ahamad and A. K. Tiwari, *Int. Curr. Pharm. J.*, 2012, **1**, 110–118.
14 M. A. Ali, N. Kataoka, A.-H. Ranneh, Y. Iwao, S. Noguchi, T. Oka and S. Itai, *Chem. Pharm. Bull.*, 2017, **65**, 42–48.
15 T. K. Kwon, S. K. Hong and J.-C. Kim, *J. Ind. Eng. Chem.*, 2012, **18**, 563–567.
16 R. R. Bhosale, R. A. Osmani, B. R. Harkare and P. P. Ghodake, *Scholars Acad. J. Pharm.*, 2013, **2**, 481–486.
17 P. T. Spicer, K. L. Hayden, M. L. Lynch, A. Ofori-Boateng and J. L. Burns, *Langmuir*, 2001, **17**, 5748–5756.
18 F. D. Victorelli, L. S. Manni, S. Biffi, B. Bortot, H. H. Buzzá, V. Lutz-Bueno, S. Handschin, G. Calixto, S. Murgia and M. Chorilli, *J. Colloid Interface Sci.*, 2022, **620**, 419–430.
19 L. Boge, K. Hallstensson, L. Ringstad, J. Johansson, T. Andersson, M. Davoudi, P. T. Larsson, M. Mahlapuu, J. Håkansson and M. Andersson, *Eur. J. Pharm. Biopharm.*, 2019, **134**, 60–67.
20 T. E. Hartnett, A. J. O'Connor and K. Ladewig, *Expert Opin. Drug Delivery*, 2015, **12**, 1513–1526.
21 Q. Chai, Y. Jiao and X. Yu, *Gels*, 2017, **3**, 6.
22 V. Karthika, P. Sheri and M. Kuriachan, *Int. J. Res. Rev.*, 2018, **5**, 149–159.
23 A. Adak, V. Castelletto, A. de Sousa, K.-A. Karatzas, C. Wilkinson, N. Khunti, J. Seitsonen and I. W. Hamley, *Biomacromolecules*, 2024, **25**, 1205–1213.
24 M. A. Iqbal, R. A. Haque, S. F. Nasri, A. A. Majid, M. B. K. Ahamed, E. Farsi and T. Fatima, *Chem. Cent. J.*, 2013, **7**, 1–17.
25 A. E. Eldeeb, S. Salah and M. Ghorab, *J. Drug Delivery Sci. Technol.*, 2019, **52**, 236–247.
26 L. M. Ahmed, K. M. Hassanein, F. A. Mohamed and T. H. Elfaham, *Sci. Rep.*, 2023, **13**, 17941.
27 A. Tekade, P. Ghodke, A. Patange and P. Patil, *J. Drug Delivery Sci. Technol.*, 2023, **87**, 104797.
28 A. Ramalheiro, J. L. Paris, B. F. Silva and L. R. Pires, *Int. J. Pharm.*, 2020, **591**, 119942.
29 H. M. El-Laithy, A. Badawi, N. S. Abdelmalak and N. El-Sayyad, *Chem. Pharm. Bull.*, 2018, **66**, 1165–1173.
30 K. Dua, V. R. Malipeddi, J. Madan, G. Gupta, S. Chakravarthi, R. Awasthi, I. S. Kikuchi and T. De Jesus Andreoli Pinto, *Interventional Med. Appl. Sci.*, 2016, **8**, 68–76.
31 M. A. Syed, G. Aziz, M. B. Jehangir, T. A. Tabish, A. F. Zahoor, S. H. Khalid, I. U. Khan, K. M. Hosny, W. Y. Rizg and S. Hanif, *Pharmaceutics*, 2022, **14**, 1592.
32 S. Ahmed, M. A. Kassem and S. Sayed, *Int. J. Nanomed.*, 2020, 9783–9798.
33 M. Somkiat Wattanasirichaigoon, *J. Med. Assoc. Thailand*, 2007, **90**, 724–729.
34 M. I. Asad, D. Khan, A. U. Rehman, A. Elaissari and N. Ahmed, *Nanomaterials*, 2021, **11**, 3433.
35 N. Zeghad, A. Ejaz, K. M. Zakryya, M. Aicha and B. Abdelmalik, *Curr. Issues Pharm. Med. Sci.*, 2023, **36**, 12–17.
36 A. Anis, A. Sharshar, S. El Hanbally and A. A. Shehata, *J. Clin. Med.*, 2022, **11**, 6417.
37 Q. Ou, S. Zhang, C. Fu, L. Yu, P. Xin, Z. Gu, Z. Cao, J. Wu and Y. Wang, *J. Nanobiotechnol.*, 2021, **19**, 1–12.
38 M. Atif, H. N. Bhatti, R. A. Haque, M. A. Iqbal, M. B. Ahamed Khadeer and A. M. S. A. Majid, *Appl. Biochem. Biotechnol.*, 2020, **191**, 1171–1189.
39 R. A. Haque, S. F. Nasri and M. A. Iqbal, *J. Coord. Chem.*, 2013, **66**, 2679–2692.
40 R. Y. Nadeem, M. Yaqoob, W. Yam, R. A. Haque and M. A. Iqbal, *Med. Chem. Res.*, 2022, **31**, 1783–1791.

41 M. A. Iqbal, R. Y. Nadeem, M. Yaqoob, W. Yam and R. A. Haque, *Med. Chem. Res.*, 2022, **31**, 1783–1791.
42 K. Hayat, M. Shkeel, M. A. Iqbal, M. Khalid, C. K. Quah, Q. A. Wong, A. U. Rehman, M. B. K. Ahamed, U. Farooq and S. Hameed, *Inorg. Chim. Acta*, 2023, **557**, 121694.
43 M. A. Iqbal, SSynthesis, Structure and in Vitro Anticancer Studies of Dinuclear Silver (I)-N-heterocyclic Carbene Complexes Derived from Xylyl Linked Bis-benzimidazolium Salts, PhD thesis, Universiti Sains Malaysia, 2014.
44 A. Kamal, A. H. Ibrahim, S. S. Al-Rawi, M. A. Iqbal and H. N. Bhatti, *Chem. Pap.*, 2023, 1–10.
45 G. Lei and L. Zhou, *Acta Crystallogr., Sect. E: Struct. Rep.*, 2009, **65**, o2613.
46 N. S. Goud, S. M. Ghouse, J. Vishnu, D. Komal, V. Talla, R. Alvala, J. Pranay, J. Kumar, I. A. Qureshi and M. Alvala, *Bioorg. Chem.*, 2019, **89**, 103016.
47 U. B. Suleiman, U. Yunusa, A. Muhammad and M. B. Ibrahim, *Port. Electrochim. Acta*, 2023, 363–380, DOI: **10.4152/pea.2023410504**.
48 A. Chakraborty, S. Debnath, T. Ghosh, D. K. Maiti and S. Majumdar, *Tetrahedron*, 2018, **74**, 5932–5941.
49 N. F. Younes, S. A. Abdel-Halim and A. I. Elassasy, *Int. J. Pharm.*, 2018, **553**, 386–397.
50 A. B. Cintra, L. A. Delboni and M. G. Lara, *Braz. J. Pharm. Sci.*, 2023, **58**, e20803.
51 X. Pan, K. Han, X. Peng, Z. Yang, L. Qin, C. Zhu, X. Huang, X. Shi, L. Dian and M. Lu, *Curr. Pharm. Des.*, 2013, **19**, 6290–6297.
52 V. K. Rapalli, S. Banerjee, S. Khan, P. N. Jha, G. Gupta, K. Dua, M. S. Hasnain, A. K. Nayak, S. K. Dubey and G. Singhvi, *Mater. Sci. Eng., C*, 2021, **119**, 111548.
53 W. S. Alharbi and K. M. Hosny, *J. Drug Delivery Sci. Technol.*, 2020, **57**, 101710.
54 F. Hashem, M. Nasr and M. Youssif, *J. Adv. Pharm. Res.*, 2018, **2**, 95–103.
55 K. C. Achar, K. M. Hosamani and H. R. Seetharamareddy, *Eur. J. Med. Chem.*, 2010, **45**, 2048–2054.
56 H. A. Elgendy, A. M. Makky, Y. E. Elakkad, R. M. Ismail and N. F. Younes, *Drug Deliv.*, 2023, **30**, 2162159.
57 A. Sanjana, M. G. Ahmed and J. G. BH, *Mater. Today: Proc.*, 2022, **50**, 197–205.
58 S. S. Patil, K. Roy, B. Choudhary and K. R. Mahadik, *Drug Dev. Ind. Pharm.*, 2016, **42**, 1300–1307.
59 A. A. El-Shenawy, M. M. Elsayed, G. M. Atwa, M. A. Abourehab, M. S. Mohamed, M. M. Ghoneim, R. A. Mahmoud, S. A. Sabry, W. Anwar and M. El-Sherbiny, *Pharmaceutics*, 2023, **15**, 680.
60 A. Zerriouh, A. Deghiche, W. Bououden, D. Cavallo, F. Rainone, A. Erto and N. Haddaoui, *J. Mol. Liq.*, 2023, **382**, 121914.
61 Z. Chen, Q. Huang, Y. Song, X. Feng, L. Zeng, Z. Liu, X. Hu, C. Tao, L. Wang and Y. Qi, *Biomed. Pharmacother.*, 2023, **166**, 115316.
62 D. C. A. Putri, R. Dwiastuti and A. K. N. Marchaban, *J. Farm. Sai. Komun.*, 2017, **14**, 79–85.
63 M. Nasr, H. Younes and R. S. Abdel-Rashid, *Drug Delivery Transl. Res.*, 2020, **10**, 1302–1313.
64 M. Sakhi, A. Khan, I. Khan, S. A. Khan, S. I. Khan, M. A. Khattak, M. N. Uddin, M. Kazi and F. Nasir, *Saudi Pharm. J.*, 2023, **31**, 101697.
65 R. M. Zaki, A. El Sayeh Abou El Ela, A. S. Almurshedi, B. N. Aldosari, A. A. Aldossari and M. A. Ibrahim, *Polymers*, 2023, **15**, 1774.
66 H. A. El-Enin and A. H. Al-Shanbari, *Saudi Pharm. J.*, 2018, **26**, 790–800.
67 K. Prabahar, U. Uthumansha, N. Elsherbiny and M. Qushawy, *Pharmaceuticals*, 2023, **16**, 563.
68 N. Mukherjee, S. Ghosh, J. Sarkar, R. Roy, D. Nandi and S. Ghosh, *ACS Appl. Mater. Interfaces*, 2023, **15**, 33457–33479.
69 S. Sen, S. Ghosh, A. Jana, M. Jash, S. Ghosh, N. Mukherjee, D. Mukherjee, J. Sarkar and S. Ghosh, *ACS Appl. Bio Mater.*, 2024, **7**(6), 4142–4161.
70 A. M. Al-Mahallawi, A. A. Abdelbary and S. A. El-Zahaby, *Int. J. Pharm.*, 2021, **600**, 120490.
71 N. Mukherjee, S. Ghosh, R. Roy, D. Mukherjee, S. Sen, D. Nandi, J. Sarkar and S. Ghosh, *ACS Appl. Mater. Interfaces*, 2024, 30929–30957.
72 S. M. Arman and C. Mark-Herbert, *Sustainability*, 2021, **13**, 10242.
73 A. Adak, V. Castelletto, B. Mendes, G. Barrett, J. Seitsonen and I. W. Hamley, *ACS Appl. Bio Mater.*, 2024, **7**(8), 5553–5565.
74 U. Rehman, A. Sheikh, A. Alsayari, S. Wahab and P. Kesharwani, *Colloids Surf., B*, 2023, 113728.